Satellite Passive Microwave Rain Rate Measurement over Croplands during Spring, Summer and Fall

ROY W. SPENCER[1]

Space Science and Engineering Center, University of Wisconsin-Madison, Madison, WI 53706

(Manuscript received 28 March 1984, in final form 11 August 1984)

ABSTRACT

Rain rate algorithms for spring, summer and fall that have been developed from comparisons between the brightness temperatures measured by the Nimbus-7 Scanning Multichannel Microwave Radiometer (SMMR) and rain rates derived from operational WSR-57 radars over land are described. Data were utilized from a total of 25 SMMR passes and 234 radars, resulting in ~12 000 observations of ~1600 km^2 areas. Multiple correlation coefficients of 0.63, 0.80 and 0.75 are achieved for the spring, summer and fall algorithms, respectively. Most of this information is in the form of multifrequency contrast in brightness temperature, which is interpreted as a measurement of the degree to which the land-emitted radiation is attenuated by the rain systems. The SMMR 37 GHz channel has more information on rain rate than any other channel. By combining the lower frequency channels with the 37 GHz observations, variations in land and precipitation thermometric temperatures can be removed, leaving rain attenuation as the major effect on brightness temperature. Polarization screening at 37 GHz is found to be sufficient to screen out cases of wet ground, which is only important when the ground is relatively vegetation free. Heavy rain cases are found to be a significant part of the algorithms' success, because of the strong microwave signatures (low brightness temperatures) that result from the presence of precipitation-sized ice in the upper portions of heavily precipitating storms. If IR data are combined with the summer microwave data, an improved (0.85) correlation with radar rain rates is achieved.

1. Introduction

The remote sensing of rainfall from satellites has, most commonly, been attempted with visible and infrared (IR) observations. These techniques rely on the existence of some relationship between the occurrence or intensity of rainfall within a cloud and the appearance or behavior of the cloud top as observed by the satellite (Barrett and Martin, 1981). Microwave radiation at window frequencies below 40 GHz easily penetrates clouds, but not precipitation. To estimate rain rates with satellite passive microwave observations at these frequencies, the rain must have a significantly different electromagnetic signature from its surroundings, whether land or ocean. This condition is easily met over the ocean because the ocean has a relatively uniform and low brightness temperature ($T_B = \epsilon T$) due to its low emissivity ($\epsilon \sim 0.5$), while the rain has a mostly uniform and high emissivity ($\epsilon \sim 0.9$) and, thus, a high brightness temperature. Theoretical and empirical treatments of the problem have, with some differences, indicated that rain rates over the ocean are retrievable (Wilheit *et al.*, 1977; Huang and Liou, 1983; Spencer *et al.*, 1983a). Land, however, has been thought to have an emissivity that is much closer to that of rain and is more variable, due to variations in soil moisture and roughness. This results in some ambiguity between wet land surfaces and rain (e.g., Rodgers and Siddalingaiah, 1983). Even if the background were uniform, theoretical results suggested that only light rain rates would be detectable (Savage and Weinman, 1975; Weinman and Guetter, 1977).

More recently, Spencer *et al.* (1983b) documented the existence of very low 37 GHz brightness temperatures from the Nimbus-7 SMMR (Scanning Multichannel Microwave Radiometer) in conjunction with heavy thunderstorm rainfalls over land.

Low brightness temperatures were also reported by Wilheit *et al.* (1982) in aircraft overflights of tropical convection at 92 and 183 GHz. The low brightness temperatures in both cases were attributed to the presence of precipitation-size ice particles in the upper portions of the storms. The 37 GHz work led to the development of a multifrequency rain estimation algorithm based upon comparisons of rain rates from operational WSR-57 radars and the microwave observations of the SMMR over the United States during the summer (Spencer *et al.*, 1983c).

The SMMR is a ten-channel, five-frequency instrument that scans conically and thus maintains a nearly constant viewing angle of 50° at the surface of the earth (Table 1).

[1] Present affiliation: Universities Space Research Association Visiting Scientist, NASA-Marshall Space Flight Center, Huntsville, AL 35812.

TABLE 1. SMMR frequencies and instantaneous field-of-view sizes at the earth's surface. Integrated (measured) fields of view are approximately square in shape, having larger short dimensions than those listed. Horizontal (H) and vertical (V) polarizations are sampled at each frequency. This is accomplished with two radiometers at 37 GHz, and one radiometer at each of the lower frequencies, which is shared between H and V on alternating scans of the instrument. In this paper the channels and their brightness temperatures will be referred to by a combination of the frequency and polarization, e.g., H37 refers to the horizontally polarized 37 GHz brightness temperature. Further information on the Nimbus-7 SMMR instrument is contained in Gloersen and Barath (1977).

	Frequency (GHz)				
	37	21	18	10.7	6.6
Polarization	V, H	V, H	V, H	V, H	V, H
Wavelength (cm)	0.81	1.36	1.66	2.80	4.54
Instantaneous field of view (km)	18 × 27	30 × 46	41 × 55	59 × 91	95 × 148

The purpose here is to describe the development of spring and fall rain rate algorithms from SMMR and radar data comparisons, to investigate the forms of the spring, summer and fall algorithms, and to compare the microwave with infrared data in terms of rain rate information content.

2. Method

a. Radar–microwave–IR comparisons

Radar rain rates from operational WSR-57 radars were compared to SMMR brightness temperatures at full resolution to determine how much information on rain rate is contained in the SMMR observations. This was done for eight SMMR passes each during the fall of 1978 and the spring of 1979 and nine SMMR passes during the summer of 1979. These dates and times are listed in Table 2, along with the number of radars involved in the comparisons. The region of interest was east of the Rocky Mountains and west of the Appalachian Mountains, an area primarily comprised of croplands, woodlands and pasture. The analysis days were chosen by comparing the locations of SMMR swaths to radar summary charts produced hourly by the National Meteorological Center. Because the fraction of the SMMR pass covered by rain was typically small, only those cases having the most widespread rains were chosen for analysis. However, this procedure might bias the final results. Radar microfilm records were inspected for photographic quality, low elevation angles of the radar beam (generally less than 1°), presence of discernable D-VIP (digital video integrator and processor) levels and viewing times no more than 8 min different from the SMMR observation times. Those pictures deemed acceptable were registered on a 20 km grid and digitized manually. Each 20 km bin was assigned an average rain rate

$$R = \sum_{i=1}^{N} a_i r_i, \tag{1}$$

where i denotes the VIP level, a_i the area of the bin covered by the ith VIP level and r_i the average rain rate represented by that VIP level. The six reflectivity levels displayed by the WSR-57 were assigned average rain rates of 4, 17, 42, 85, 147 and 190 mm h^{-1} (NOAA, 1979). The resulting rain rates are expected to have standard errors of about ±60%.

These gridded, averaged rain rates, and original resolution SMMR T_B were converted into images on the University of Wisconsin's Man-computer Interactive Data Access System (McIDAS; Suomi *et al.*, 1983). All images were remapped to a GOES-East

TABLE 2. Dates and approximate times (GMT) of SMMR and radar coverages included in the analysis for spring, summer and fall seasons, and the number of 1600 km^2 records (containing average SMMR T_B and radar rain rates) sampled from the data for each date.

Spring 1979			Summer 1979			Fall 1978		
Time date	Radars	Records	Time date	Radars	Records	Time date	Radars	Records
0630 19 March	14	667	0645 4 May	4	236	0640 6 November	9	433
1745 29 March	12	585	1715 19 June	7	321	1730 15 November	8	466
0640 31 March	15	762	0610 21 June	8	473	0625 17 November	8	357
1710 2 April	12	606	1720 1 July	14	770	0555 27 November	8	362
0610 4 April	11	607	1800 3 July	10	550	0555 3 December	7	41
0700 18 April	8	390	0700 5 July	9	354	1735 3 December	7	317
1735 20 April	14	696	1700 5 July	7	497	1700 7 December	5	355
0600 26 April	7	440	1730 7 July	17	879	0600 9 December	4	284
			0635 9 July	9	590			

projection to facilitate comparisons with GOES IR data, which were analyzed for only the summer dates in Table 2. Because of navigation errors in the SMMR data, all images were checked and corrected (if needed) by comparing the land–water T_B differences to known coastal features. When land is viewed, the corrected locations are probably accurate to within 10 km. However, because of the SMMR viewing angle of 50°, parallax errors of ~10 km are possible in the observations of heavy thunderstorms. Errors from the radar digitization might also approach 10 km. Because of these errors, it was decided that the images of the full resolution SMMR data be sampled on a 40 km grid. A 40 km square cursor was moved across the images, and average radar rain rates, IR temperatures and SMMR T_B were computed. Data from each cursor position will hereafter be referred to as a "record". These records were then statistically analyzed with a stepwise, least-squares, multiple linear regression procedure (Dixon, 1983).

b. Raingage–microwave comparisons

For the summer dates listed in Table 2, hourly raingage totals were also compared to the SMMR brightness temperatures. Those U.S. cooperative network gages that fell within the SMMR coverage area were sampled at the time closest to the SMMR observation times. A 40 km square cursor was centered on each gage location in the SMMR images, and average SMMR T_B were computed within that cursor. Subsequent statistical analyses were carried out as described in the previous section.

3. Rain system summary

Interpretation of the results of the SMMR and radar comparisons is facilitated by a knowledge of the characteristics of the rain systems contained in the data sets. A review of the synoptic situations on each day revealed that the summer rain storms were almost always convective. The spring and fall systems were more widespread and uniform (stratiform). Figure 1 shows composited radar images, made up of the maximum rain rate at each point, of all the rain systems in the spring, summer and fall data sets. The most intense storms occurred during the summer, which is quantitatively revealed in Fig. 2 by a comparison of the frequency distribution of rain rates between the spring, summer and fall seasons. It must be remembered that these rates have been averaged over 1600 km^2 areas, and thus are, in many cases, considerably smaller than the peak rates found within the systems.

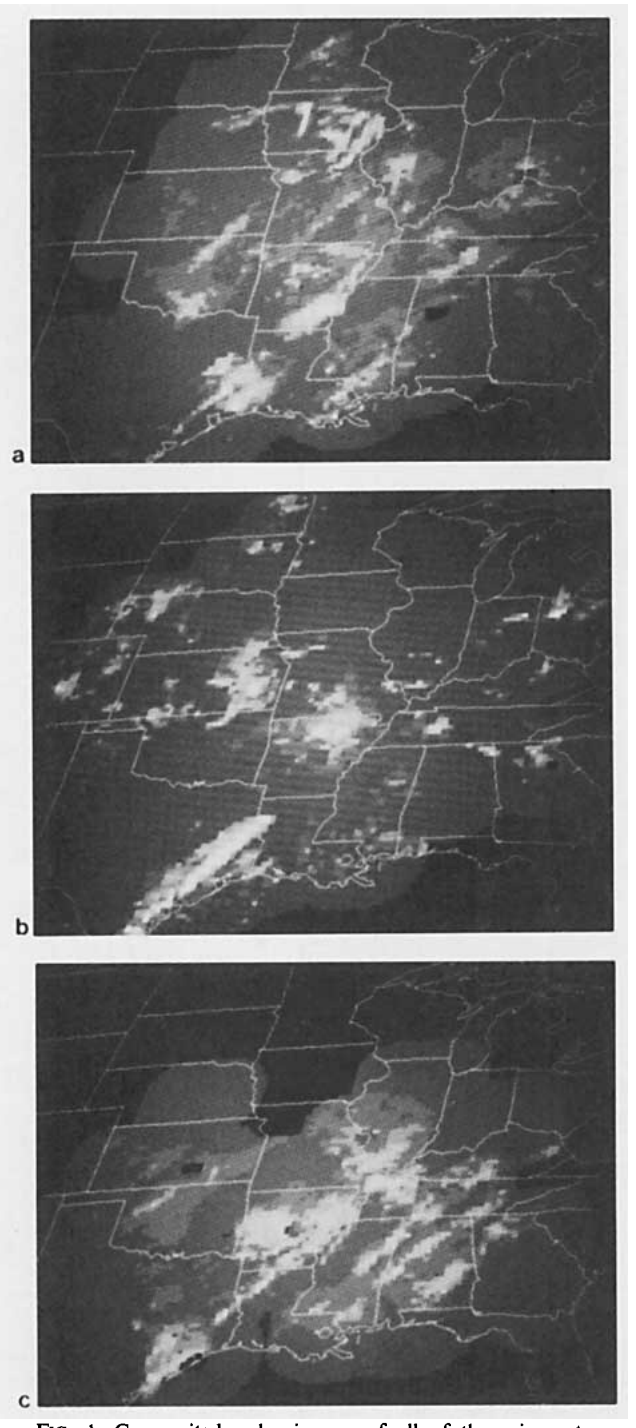

FIG. 1. Composited radar images of all of the rain systems involved in the microwave algorithm development for (a) spring, (b) summer and (c) fall at 20 km resolution. Image brightness increases linearly with rain rate from 0 mm h^{-1} (dimmest) to 88 mm h^{-1} (brightest). (b) is taken from Spencer *et al.* (1983c) and is included here for comparison.

4. The 21 June 1979 case

To illustrate the effect of rain on the different SMMR channels, Fig. 3 shows radar and vertically polarized 37, 18 and 10.7 GHz images (V37, V18, V10.7) from 0610 GMT 21 June 1979. It is obvious that, of the three SMMR images, the 37 GHz image (Fig. 3b) is the best representation of the radar image

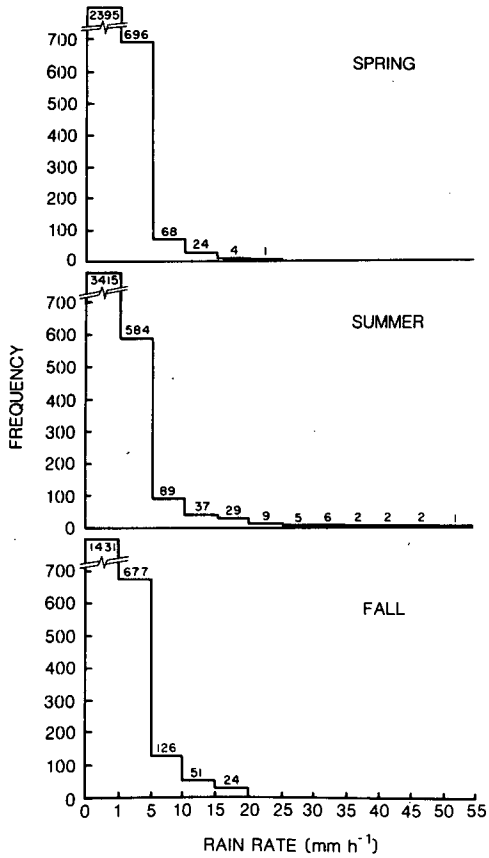

FIG. 2. Frequency histograms of the rain rates contained in the spring, summer and fall data sets. The first bar represents the zero rain rate class. Rain rates are after sampling of the data represented in Fig. 1 on a reduced resolution (40 km) grid.

(Fig. 3a). This is revealed as a negative visual correlation between rain rate and T_B, both of which vary in direct proportion to image brightness.

It can be seen from Figs. 3c and 3d that the 18 and 10.7 channels are much less affected by the rain than the 37 GHz channel is. This is because rain becomes increasingly transparent and the SMMR footprint size increases as the frequency decreases. The effect of soil and vegetation on the sensed radiation then becomes greater. Kirdiashev *et al.* (1979), Jackson *et al.* (1982) and Mo *et al.* (1982) have shown that the penetration of vegetation by microwave radiation is directly related to the moisture content of the vegetation canopy. A thick canopy of soybeans or corn, for instance, will be virtually opaque to the transfer of radiation from 37 to 6.6 GHz. Wheat, on the other hand, will be somewhat transparent at 6.6 GHz because of the sparseness and low moisture content of the cover but still will be quite opaque at 37 GHz. Thus, we might expect that the form of any multifrequency rain estimation algorithm should depend somewhat on the character of the vegetation.

5. Results

a. Radar–microwave comparisons

1) DATA SCREENING

Initially data were screened to remove those observations of 1) oceans, lakes or wet soil surfaces and 2) land surfaces having higher T_B than any rain cell in the data sample. As noted by Weinman and Guetter (1977), wet soil and water bodies can be distinguished from rain by their large values of 37 GHz polarization. [The term "polarization" in this paper, when not accompanied by a modifier, refers to the difference between the vertically and horizontally polarized brightness temperatures ($T_B^V - T_B^H$) at a single frequency.] They suggested correcting the brightness temperatures by an amount proportional to the polarization value. This was tried with the current data set, but a simple screening procedure was found to be slightly more effective. The screening was based upon measurements from the data sets in Table 2 indicating that 37 GHz observations of rainclouds on a 40 km scale almost never have polarizations exceeding 16°C over land. Individual SMMR 37 GHz observations (27 km resolution) reveal that the cores of intense storms have even larger polarizations, exceeding 20° when H37 falls below 175 K, but the 40 km sampling results in polarizations generally below 16°C. This increase in polarization with increasing storm intensity might be related to the shape and orientation of ice particles in the upper portions of storms. The 37 GHz observations of water and wet soil were found to have polarizations far exceeding 16°C, with increasing polarization indicating increasing moisture content and/or reduced vegetative cover.

An additional screening procedure was used to exclude those records near coastal waters where the low-frequency observations, by virtue of their large footprints, were also contaminated by the water bodies. This screening took the form of H10.7 > 225 K, and was only used for the summer data. During the spring and fall this criterion excluded an unacceptably large number of cases of light rain over wet ground. Thus, for spring and fall, an alternate screening (H18 > 230 K) was utilized.

2) STRATIFIED RAIN CLASSES

After screening, the SMMR and radar-averaged data (records) were grouped into rain intensity intervals: zero, 1 to 10, 11 to 20 (and in the case of the summer data), 21 to 30 and >30 mm h^{-1}. The average values of SMMR T_B's at various frequencies for each of these rain rate intervals are shown in Fig. 4a for the horizontal polarizations and Fig. 4b shows those for the vertical polarizations. It is apparent from both charts that the brightness temperatures for the first three rain intervals are warmest during the summer. At $R = 0$, the obvious reason for this is that the warmest land surfaces occur during the

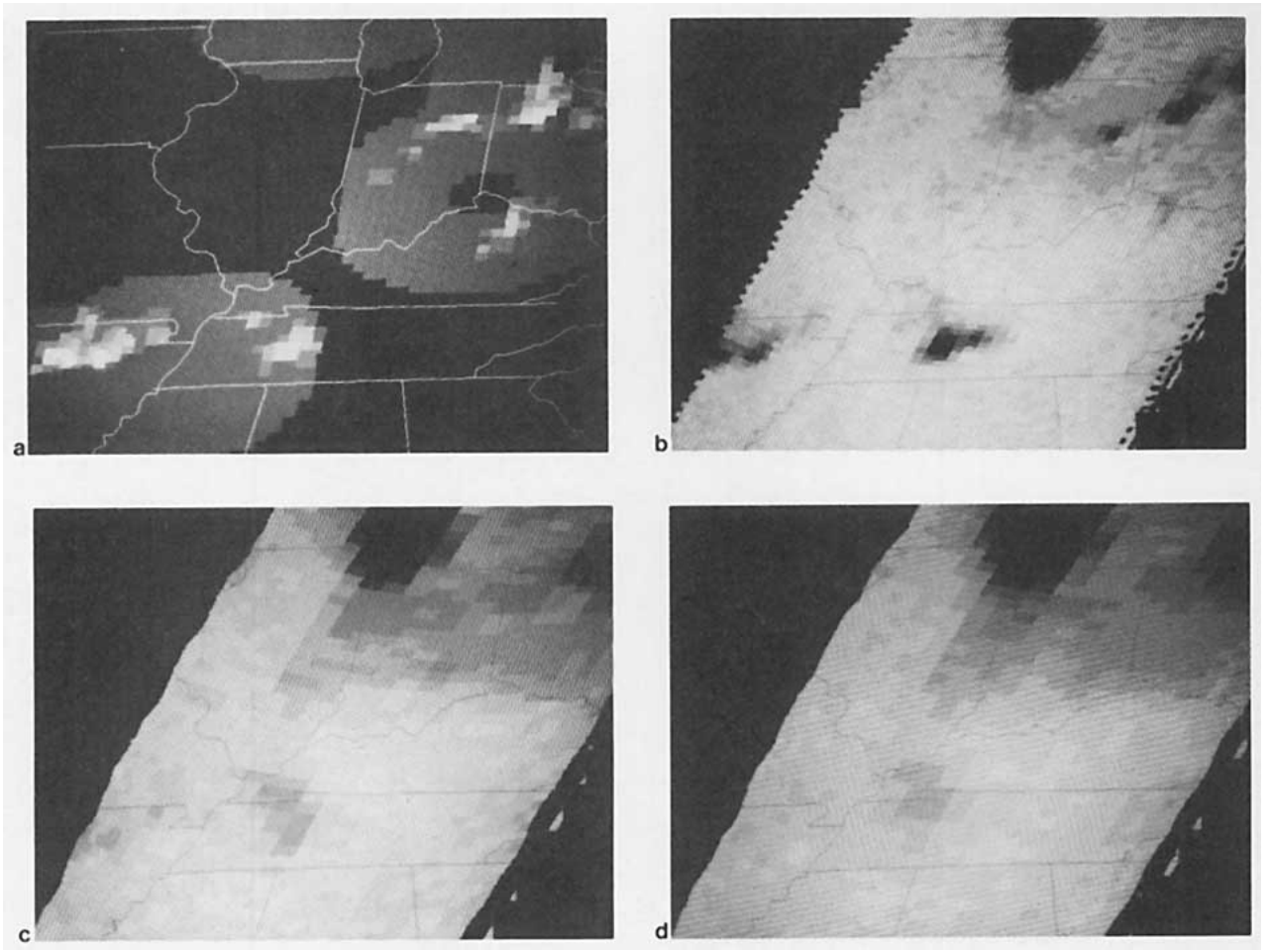

FIG. 3. Images of (a) radar rain rate, (b) V37 T_B, (c) V18 T_B and (d) V10.7 T_B at 0610 GMT 21 June 1979 over the eastern United States. The radar rain rates range up to 76 mm h^{-1} while the 37 GHz T_B range as low as 206 K.

summer. This variation in land temperature has important implications. Note that at 37 GHz, the average T_B for rain-free areas during spring and fall corresponds to a rain rate of approximately 6 mm h^{-1} during the summer. At 21 GHz this increases to 14 mm h^{-1}. Thus, seasonal (as well as synoptic) changes in the land–atmosphere thermometric temperatures can adversely affect microwave rain estimates if they are not taken into account in some way.

Note also that the T_B drop off most at the lower frequencies during the spring, and least during the summer. This is a result of the seasonal variations in vegetative cover and soil moisture. The spring data set contains the most observations of bare or partially covered soil, the moisture content of which leads to a lower emissivity and thus lower T_B. Additional evidence of this is shown in Fig. 5, which gives a seasonal plot of the values of polarization for the $R = 0$ class. It can be seen that the spring land observations have the highest values of polarization, due to the flat and moist character of the soil compared to that of the vegetated surfaces of fall, and especially, summer. Specific examples of these differences are illustrated in Fig. 6, the effective emissivities of partly flooded soil, moist soil, mature corn fields, forest and Amazon jungle at 37, 18 and 6.6 GHz. The effective emissivities of all of the vegetated surfaces are essentially the same (to within the accuracy allowed by the estimation of temperatures with GOES-East IR data), while those of the exposed moist partially flooded soil surfaces are lower, especially at the lower frequencies. Thus, well-vegetated surfaces provide a uniform background to which the rain cell brightness temperatures can be compared, with little ambiguity due to emissivity variations of the land surface. Partly flooded, exposed soils will be screened out by the 37 GHz polarization screening (e.g., the bottom curve in Fig. 6). However, the exposed soils that may be moist within but not moist enough on the surface to result in large 37 GHz polarizations remain a complicating factor due to greater variations in the lower frequency T_B as the soil moisture varies.

As we inspect the SMMR T_B for the second and

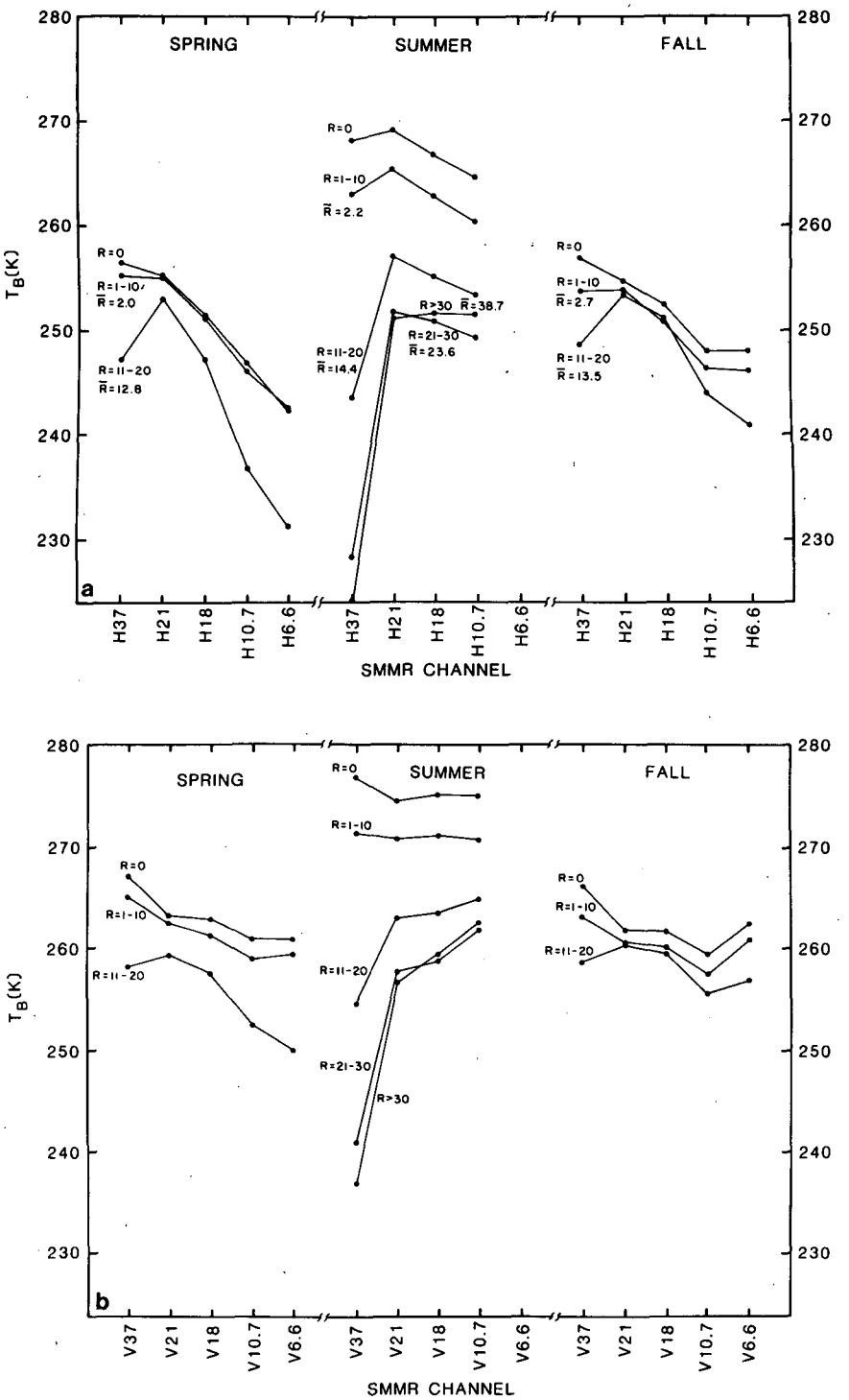

FIG. 4. Average SMMR (a) horizontally polarized and (b) vertically polarized brightness temperatures for different rain rate classes and different seasons. Each class's average T_B are represented as a series of connected dots and labeled with the rain rate interval and average rain rate for that class (in mm h^{-1}).

third rain classes (1 to 10 and 11 to 20 mm h^{-1}) in Fig. 4, we note that the summer classes appear to be the most separable from the $R = 0$ class. The two heaviest rain classes (21 to 30 and >30 mm h^{-1}) are even more separable from the $R = 0$ class, especially at 37 GHz. A curious result is that the $R > 30$

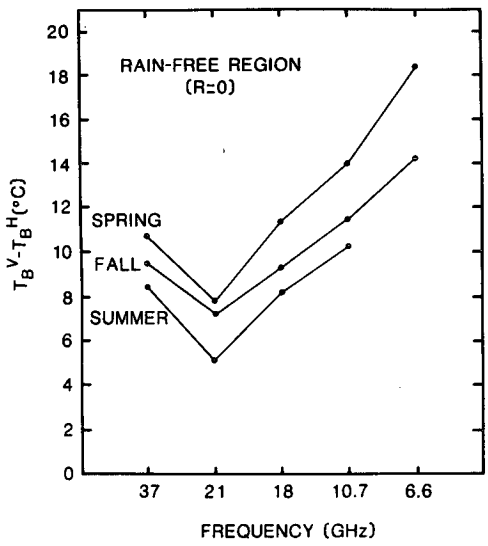

FIG. 5. Average values of polarization ($T_B^V - T_B^H$) for the different frequencies and seasons in rain-free areas illustrating the effects that seasonal variations in soil moisture and vegetative cover have on the observed brightness temperatures.

summer curve is actually warmer at 18 and 10.7 GHz than that of the preceding rain class. This may be due to warmer synoptic conditions that may have attended the storms of the heaviest rain class. In stark contrast to this behavior is the bottom spring curve, which reveals a marked T_B drop at 10.7 and 6.6 GHz at the heaviest rain class. This is most easily interpreted as a result of wetting of the spring soils during the heavier rainfalls. These wet soils were not screened out at 37 GHz because the heavy rain is opaque at 37 GHz, but not at 10.7 and 6.6 GHz.

3) REGRESSION EQUATIONS

A stepwise multiple linear-regression procedure was utilized to derive equations relating the radar rain rate to a linear combination of SMMR brightness temperatures. Nonlinear regression was tried on the summer data set, but the results were not significantly improved. The regression equations that resulted from the statistical analysis of SMMR T_B versus radar rain rates (after screening) are listed in Table 3, along with their performance in terms of multiple correlation (r) and the explained variance of the radar data (r^2). Using these correlation measures, the summer equation has the best performance ($r = 0.795$), the fall is a close second ($r = 0.752$) and the spring is a rather distant third ($r = 0.625$). One of the most evident characteristics of these equations is the *similarity of the signs* of the coefficients between seasons. Note that all 37 GHz terms have negative coefficients, as do five of the six 10.7 GHz terms, but all 21 and 18 GHz terms have positive coefficients. This is an interesting result in light of the fact that *all* channels for *all* three seasons were, individually, *negatively* correlated with radar rain rate. These differing coefficient signs can be explained by synoptic and seasonal variations in thermometric temperatures. The equations show that the rain rate is, to a first approximation, proportional to the difference between the 37 GHz T_B and the 21 and 18 GHz T_B. If the thermometric temperature of the observed rain–atmosphere–land system never varied, we would only need one frequency to observe the rain-induced attenuation effects (primarily scattering) that are related to rain rate. However, these thermometric temperatures do vary. Thus, at least two channels are needed to remove those variations and isolate the scattering mechanism, which varies considerably with wavelength (stronger at the shorter wavelengths). There may be additional explanations that are not immediately obvious for these coefficient differences. The negative coefficients on the 10.7 GHz terms might represent additional rain-attenuation information that

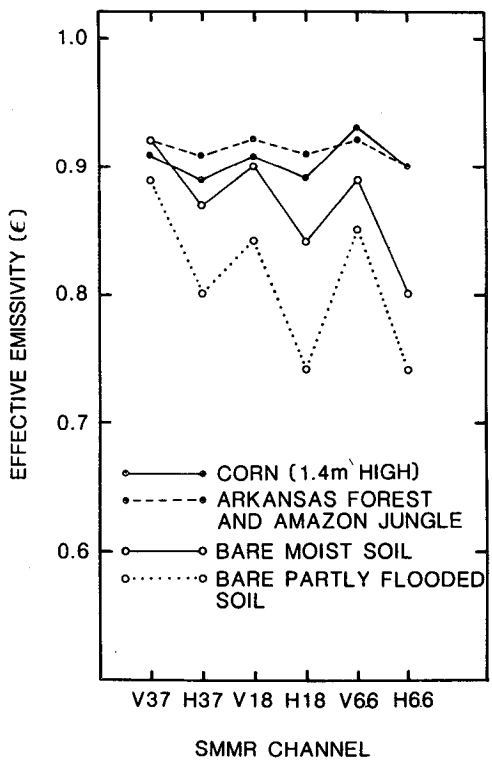

FIG. 6. Effective emissivities (SMMR T_B/surface thermometric temperature) of different surfaces. The corn data was sampled on 9 July 1979 over west-central Iowa. The corn canopy averaged 1.4 m in height. The forest data were sampled at the same time over west-central Arkansas. The Amazon jungle data were sampled from a 1.5×10^4 km^2 area centered at 8°S, 56°W in Brazil on 5 July 1979. The mostly unvegetated moist soils were sampled over south-central Iowa on 31 March 1979, while the partly flooded mostly unvegetated soils were sampled over north-central Iowa at the same time. Crop and moisture characteristics were provided by the United States Department of Agriculture (1979).

TABLE 3. SMMR rain rate regression equations and their performance for spring, summer and fall. For the summer the data must satisfy the following criteria: (V37 − H37) ≤ 16°C and H37 < 280 K and H10.7 > 225 K. For the spring and fall the data must satisfy: (V37 − H37) ≤ 16°C and H18 > 230 K. The total number of records before screening/after screening are: spring (4753/3031), summer (4663/3782) and fall (2615/2288).

		SMMR channel T_B coefficients											
	Constant	H37	V37	H21	V21	H18	V18	H10.7	V10.7	H6.6	V6.6	r	r^2
Spring	38.3	−0.107	−0.442	0.279	0.119	0.107	0.105	−0.109	−0.121	×	0.034	0.625	0.391
Summer	32.6	−0.408	−0.378	0.215	0.137	0.406	0.090	−0.242	0.062	*	*	0.795	0.631
Fall	49.9	−0.157	−0.789	0.437	0.261	0.055	0.258	−0.136	−0.102	×	×	0.752	0.565

* Not included in the analysis.
× Not chosen by the regression procedure.

is not contained in the 37 GHz measurements. This is quite possible because the upper portions of the rain layer are sampled at 37 GHz, while the 10.7 GHz measurements have their contribution from much lower in the rain layer. Either reduction of noise in the measurements or additional physical processes that have not been accounted for and are not immediately apparent can explain the large number of channels included in the equations.

Figure 7 illustrates the relative importance of each regression step in reducing the unexplained variance of the rain rates. For the spring, summer and fall equations we see that the 37 and 21 GHz channels (the first two regression steps) provide most of the available information on rain rates. The choice of 21 GHz data in the second regression step for each equation supports the explanation that thermometric temperature variations are implicitly being accounted for, since the 21 GHz channel is quite sensitive to water vapor and thus to the temperature of the atmosphere.

It is of considerable interest to know what effect heavier rain cases in the summer data have on the algorithm performance. If only those records that have $R < 20$ are analyzed, about 4% of the nonzero rain cases are omitted, but the explained variance is reduced by 11% (the dotted curve in Fig. 7). Therefore, the heavier rain cases are significant contributors to the success of the summer microwave algorithm. The poorer performance of this modified summer equation (restricted to light rain rates) compared to the fall equation is probably a result of radar-derived rain

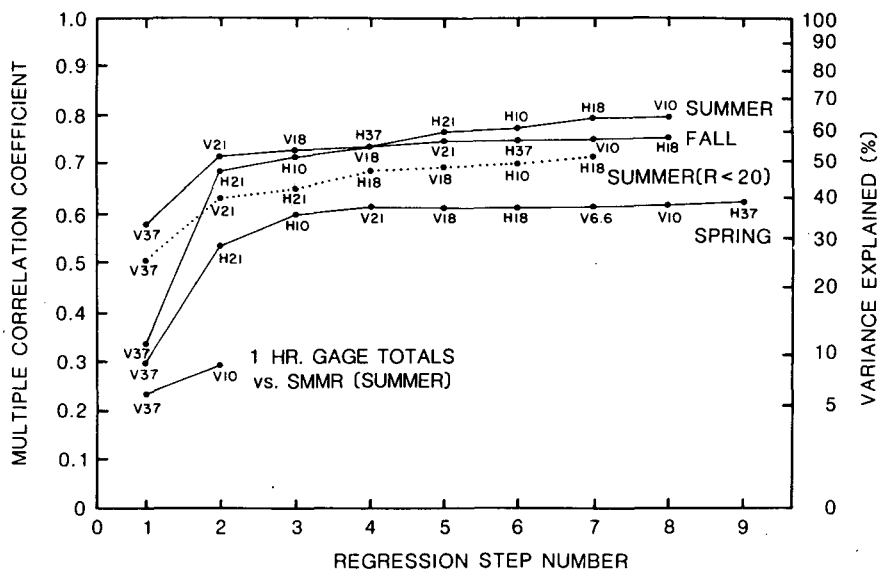

FIG. 7. The multiple correlation and explained variance achieved at each regression step in the derivation of the spring, summer and fall equations. The channels chosen by the regression procedure are shown at each step. The dotted line represents the summer equation that results if the analysis is restricted to rain rates less than 20 mm h^{-1}. The short line at the bottom shows the correlations achieved if the summer T_B are compared to 1307 U.S. cooperative network raingages. The summer solid line does not cross the fall line at step 4.

rate accuracy. The fall radar microfilm images had a better overall quality than those of summer.

As reported by Spencer *et al.* (1983c), the summer equation was tested on an independent data set (one SMMR pass, 13 radars) with a virtually identical correlation (0.80) to that of the dependent data set with rain rate (0.79). Independent tests of the spring and fall algorithms were not performed.

b. Gage–microwave comparisons

If one-hour raingage totals rather than the radar rates are compared to the SMMR data, the correlations are greatly diminished. In Fig. 7 we see that only two steps were completed by the regression, with only 9% of the variance of the gage totals being explainable by the SMMR T_B. Such a poor result can be partly attributed to the poor correlation of one-hour gage totals with rain rates averaged over a 1600 km^2 area. This is supported by a correlation of 0.299 between the radar rates and the gage totals. A virtually identical correlation exists between the SMMR gage algorithm and the gage totals (0.294).

c. Radar–IR comparisons

The GOES-East IR temperatures also were found to contain significant information on rain rate during the summer. From the 4663 comparisons of radar and IR data (averaged over 1600 km^2 areas) it was found that rain never occurred when IR temperature exceeded 280 K. The comparisons also showed that the relationship between IR temperature and radar rain rate is highly nonlinear. The rain rates were compared to different powers of (280 K − IR) to find an optimal functional relationship between the two types of data (Fig. 8). Note that 46% of the radar variance can be explained by a 12th power of (280 K − IR). This compares to 21% of the variance with only a linear comparison to IR. The nonlinearity arises because of an unbalanced situation whereby significant rains cannot occur in the absence of cold clouds but cold clouds can occur in the absence of significant rains. In contrast to this situation, microwave observations of low, unpolarized 37 GHz brightness temperatures will often occur in the presence of significant rains, and heavy rains will almost always be associated with low brightness temperatures. Thus, a strong IR signature (very low temperature) will have a larger ambiguity concerning the location and intensity of rain than will a strong microwave signature (very low T_B).

If microwave screening is combined with IR screening (IR < 280 K) and then IR terms are entered into the regression procedure along with the SMMR T_B, an improved rain rate equation results (Table 4). The explained radar variance increases from 63% for the microwave-only equation to nearly 73% with IR screening and IR terms. This improvement (10%) is attributable to only a crude treatment of the IR data, and further improvement might be expected with a more detailed treatment. This improvement seems to indicate that there is additional information in the IR observations that is not contained in the microwave data. Thus, the infrared data can be thought of as a useful addition to the precipitation measurement scheme, at least in convective situations.

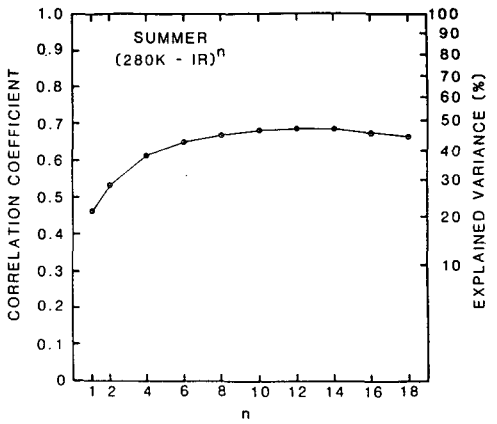

FIG. 8. The explained variance of the radar rain rates as a function of the power to which the GOES-East IR temperatures are raised. Only those temperatures less than 280 K are included in the analysis, resulting in 2040 records from the summer data set.

6. Summary and conclusions

The passive microwave observations of the Nimbus-7 SMMR have significant and useful information on radar-derived rain rates over the United States during summer and fall. During spring there is also significant information, but the influence of nonvegetated moist ground on the land-background brightness temperatures results in a poor multifrequency contrast between light rain systems and their surroundings. A linear combination of most of the SMMR channels (37, 21, 18, 10.7 GHz) provides this information on rain rate. The 37 and 21 GHz channels contain most of the information needed to explain the variance of the radar rates, while the 18 and 10.7 GHz provide significant, but smaller improvements.

The rain rate is closely related to the difference between the 37 GHz T_B and the 21 and 18 GHz T_B. This difference is interpreted as a measure of the degree to which the rain attenuates the upwelling environmental radiation. The effect that thermometric temperature variations have on T_B is thus removed, isolating the scattering that is due to the rain and, especially, to the precipitation-sized ice overlying the rain. Because vegetative cover (and thus the amount of exposed soil) changes seasonally, different equations are used to improve performance within seasons. The

TABLE 4. Combined SMMR and GOES-East IR rain rate regression equation for the summer season. Data had to satisfy four requirements: IR < 280 K, V37 − H37 ≤ 16°C, H37 < 280 K and H10.7 > 225 K. The multiple correlation (r) and explained variance (r^2) are shown at each regression step.

	Regression step number								
	0	1	2	3	4	5	6	7	8
Variable		V37	V21	$(280\ K - IR)^{12}$	H21	H37	H18	H10	V18
Coefficient	35.3	−0.324	0.120	3.46×10^{-22}	0.107	−0.335	0.398	−0.188	0.094
Multiple r		0.711	0.796	0.832	0.837	0.842	0.846	0.852	0.853
Multiple r^2		0.505	0.633	0.692	0.700	0.708	0.715	0.726	0.728

results are much poorer if raingages are used as ground truth. This is probably due to the poor correspondence between 1 h gage totals and the instantaneous rain rate over a large area. If GOES-East IR data are pooled with the summer microwave data, a 10% increase (to 73%) in the explained variance of the radar rain rates is attained.

It is concluded that passive microwave rain rate estimation over land surfaces is possible, especially when the land background has a relatively constant emissivity. This condition is met most of the time in middle latitudes during the warm season and in much of the tropics year round, when vegetation covers the surface. Vegetation wetting by dew or rain appears to have little effect on emissivity, since that wetting is in the form of a relatively few number of spheroidal droplets spread over a thin layer. The effect of precipitation-sized ice particles is to reduce the 37 GHz T_B greatly in the presence of heavy rain, and thus improve the rain signal-to-land noise ratio.

Acknowledgments. I am grateful to Drs. Barry Hinton, David Martin and Norman Grody for their helpful comments during portions of this research, and especially to David Santek for his invaluable assistance with McIDAS. Angela Crowell typed the manuscript. Financial support was provided by NOAA/NESDIS under Contract NA-80-SAC-00742.

REFERENCES

Barrett, E. C., and D. W. Martin, 1981: *The Use of Satellite Data in Rainfall Monitoring.* Academic Press, 340 pp.

Dixon,W. J., Ed., 1983: *BMDP Statistical Software.* University of California Press.

Gloersen, P., and F. T. Barath, 1977: A scanning multichannel microwave radiometer for Nimbus-G and Seasat-A. *IEEE J. Oceanic Eng.,* **OE-2,** 172–178.

Huang, R., and K.-N. Liou, 1983: Polarized microwave radiation transfer in precipitating cloudy atmospheres: Applications to window frequencies. *J. Geophys. Res.,* **88,** 3885–3893.

Jackson, T. J., T. J. Schmugge and J. R. Wang, 1982: Passive microwave sensing of soil moisture under vegetation canopies. *Water Resour. Res.,* **18,** 1137–1142.

Kirdiashev, K. P., A. A. Chukhlantsev and A. M. Shutko, 1979: Microwave radiation of the earth's surface in the presence of vegetation cover. *Radio Eng. Electron. Phys.* (Engl. Transl.,) **24,** 256–264.

Mo, T., B. J. Choudhury, T. J. Schmugge, J. R. Wang and T. J. Jackson, 1982: A model for microwave emission from vegetation-covered fields. *J. Geophys. Res.,* **87,** 11 229–11 237.

NOAA, 1979: *Introduction to Weather Radar.* U.S. Dept. of Commerce, 70 pp.

Rodgers, E., and H. Siddalingaiah, 1983: The utilization of Nimbus-7 SMMR measurements to delineate rainfall over land. *J. Climate Appl. Meteor.,* **22,** 1753–1763.

Savage, R. C., and J. A. Weinman, 1975: Preliminary calculations of the upwelling radiance from rainclouds at 37.0 and 19.35 GHz. *Bull. Amer. Meteor. Soc.,* **56,** 1272–1274.

Spencer, R. W., B. B. Hinton and W. S. Olson, 1983a: Nimbus-7 37 GHz radiances correlated with radar rain rates over the Gulf of Mexico. *J. Climate Appl. Meteor.,* **22,** 2095–2099.

——, W. S. Olson, W. Rongzhang, D. W. Martin, J. A. Weinman and D. A. Santek, 1983b: Heavy thunderstorms observed over land by the Nimbus-7 scanning multichannel microwave radiometer. *J. Climate Appl. Meteor.,* **22,** 1041–1046.

——, D. W. Martin, B. B. Hinton and J. A. Weinman, 1983c: Satellite microwave radiances correlated with radar rain rates over land. *Nature,* **304,** 141–143.

Suomi, V. E., R. Fox, S. S. Limaye and W. L. Smith, 1983: McIDAS III: A modern interactive data access and analysis system. *J. Climate Appl. Meteor.,* **22,** 766–778.

USDA, 1979: *Weekly Weather and Crop Bulletin.* U.S. Dept. of Commerce, **66,** No. 29, 23 pp.

Weinman, J. A., and P. J. Guetter, 1977: Determination of rainfall distributions from microwave radiation measured by the Nimbus-6 ESMR. *J. Appl. Meteor.,* **16,** 437–442.

Wilheit, T. T., A. T. C. Chang, M. S. V. Rao, E. B. Rodgers and J. S. Theon, 1977: A satellite technique for quantitatively mapping rainfall rates over the oceans. *J. Appl. Meteor.,* **16,** 551–560.

——, ——, J. L. King, E. B. Rodgers, R. A. Nieman, B. M. Krupp, A. S. Milman, J. S. Stratigos and H. Siddalingaiah, 1982: Microwave radiometric observation near 19.35, 92, and 183 GHz of precipitation in Tropical Storm Cora. *J. Appl. Meteor.,* **21,** 1137–1145.